High-resolution photoelectron imaging of cold C 60 − anions and accurate determination of the electron affinity of C60

Dao-Ling Huang, Phuong Diem Dau, Hong-Tao Liu, and Lai-Sheng Wang

Citation: The Journal of Chemical Physics **140**, 224315 (2014); doi: 10.1063/1.4881421
View online: http://dx.doi.org/10.1063/1.4881421
View Table of Contents: http://scitation.aip.org/content/aip/journal/jcp/140/22?ver=pdfcov
Published by the AIP Publishing

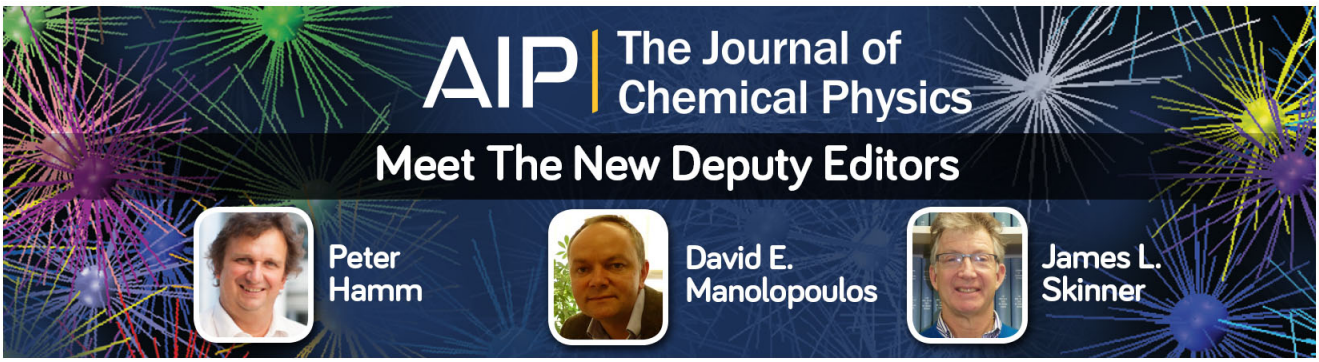

High-resolution photoelectron imaging of cold C_{60}^- anions and accurate determination of the electron affinity of C_{60}

Dao-Ling Huang, Phuong Diem Dau, Hong-Tao Liu, and Lai-Sheng Wang[a)]
Department of Chemistry, Brown University, Providence, Rhode Island 02912, USA

(Received 27 April 2014; accepted 21 May 2014; published online 11 June 2014)

High-resolution photoelectron imaging and spectroscopy of cold C_{60}^- anions are reported using a newly built photoelectron imaging apparatus coupled with an electrospray ionization source and a temperature-controlled cryogenic ion trap. Vibrationally resolved photoelectron spectra are obtained for the detachment transition from the ground state of C_{60}^- to that of C_{60} at various detachment wavelengths from 354.84 nm to 461.35 nm. The electron affinity of C_{60} is accurately measured to be 2.6835 ± 0.0006 eV. Numerous unexpected vibrational excitations are observed in the photoelectron spectra due to the Jahn-Teller effect in C_{60}^- and Hertzberg-Teller vibronic coupling in both C_{60}^- and C_{60}. Both the relative intensities of vibrational peaks and their photoelectron angular distributions provide evidence for the vibronic couplings. The observed *p*-wave-like behavior in the angular distribution of the 0_0^0 transition suggests that the electron is detached from an *s*-type orbital. © *2014 AIP Publishing LLC*. [http://dx.doi.org/10.1063/1.4881421]

I. INTRODUCTION

The C_{60} fullerene with the highest point-group symmetry (I_h) is a fascinating molecule.[1] Because of its unique electronic and structural properties, it has been considered for potential applications in molecular electronics.[2–4] The electron affinity (EA) of C_{60} is a fundamental physical property, important to its many applications. However, it had been challenging to accurately measure the EA of C_{60},[5–8] primarily because of the difficulty in creating cold C_{60}^- anions. Over the past two decades, the EA of C_{60} has been reported several times, but the accurate value is still in debate. Yang *et al.* first estimated the EA of C_{60} to be 2.6–2.8 eV from low resolution photoelectron spectroscopy (PES) of C_{60}^- in 1987.[5] Wang *et al.* improved it to be 2.65 ± 0.05 eV using threshold photodetachment and a tunable dye laser.[6] The accuracy of this study was limited because of thermionic emission of C_{60}^- that prevented the observation of a clear detachment threshold. Brink *et al.* carried out a photodetachment experiment utilizing a heavy ion storage ring and reported a highly accurate EA of 2.666 ± 0.001 eV.[9] However, this accuracy was questionable because of uncertainty in the anion temperature and the very low signal-to-noise ratio near the detachment threshold. In the meantime, a new PES experiment by Gantefor and co-workers reported an EA of 2.70 ± 0.05 eV for C_{60}.[10]

We conducted a higher resolution PES study of room-temperature C_{60}^- produced from an electrospray ionization (ESI) source with partial vibrational resolution and reported a more accurate EA of 2.689 ± 0.008 eV for C_{60}.[8] The EA was determined straightforwardly from the resolved 0_0^0 vibrational transition in the PE spectra. We subsequently refined this value to 2.683 ± 0.008 eV by performing PES of C_{60}^- cooled to 70 K in a temperature-controlled cryogenic ion trap, which completely eliminated vibrational hot bands in the PES.[11] However, a recent remeasurement of the EA of C_{60} in a cold ion storage ring, similar to that of Ref. 9, yielded a value of 2.664 ± 0.005 eV,[12] which clearly has no overlap with our previous measurement of 2.683 ± 0.008 eV using vibrationally resolved PES of cold C_{60}^-.[11] This persistent discrepancy is troubling, suggesting that the uncertainty was underestimated in either the PES or the storage ring experiment.

Because of its high symmetry, C_{60} has only 46 vibrational modes for its 174 vibrational degrees of freedom.[13–15] Extensive experimental research has been done on the vibrational spectroscopy of C_{60} in the condensed phase,[15–18] while it has been much more difficult for gaseous C_{60}. All 46 vibrational modes of C_{60} in the solid state have been assigned on the basis of a variety of spectroscopic techniques, such as inelastic neutron scattering (INS), infrared (IR), and Raman spectroscopy in conjunction with theoretical calculations.[14,15,19–22] Even the 32 IR- and Raman-forbidden modes of C_{60} have been observed because of symmetry-breaking in the condensed phase.[15,16,23] Extensive *ab initio* calculations have been done for the vibrational properties of isolated C_{60} and used to compare with experimental data in the condensed phase due to the paucity of experimental data for gaseous C_{60}.[14–16,19,21,24]

In 2005, our group successfully produced cold C_{60}^- down to 70 K in a temperature-controlled ion trap with a He/H_2 buffer gas[25] and obtained partially vibrationally resolved PES spectra and a more accurate EA for C_{60} using a magnetic-bottle PES analyzer.[11] The observed vibrational excitations in the neutral ground state were interpreted qualitatively through Jahn-Teller (JT) distortions in the C_{60}^- anion.[11] The ground state of the C_{60}^- anion is $^2T_{1u}$ under the I_h symmetry of C_{60}.[26–28] This triplet degenerate electronic state is unstable as a result of the JT effect via coupling with the H_g modes.[29] Much attention has been paid to studying the JT vibronic interactions in C_{60}^- because of the significant role it plays in the electron-phonon coupling mechanism in the superconductivity of alkali doped fullerides.[10,26–28,30–34]

a)Email: Lai-Sheng_Wang@brown.edu

We have designed a PE imaging system, which replaced the magnetic-bottle electron analyzer on our first generation ESI-PES apparatus at room temperature,[35] and studied the angular distributions of photoelectrons from multiply charged anions.[36–39] We have recently developed a high-resolution PE imaging system, which can achieve electron kinetic energy resolutions down to 1.4 cm^{-1} for low energy electrons.[40,41] We have also built an improved version of our cryogenically controlled ion trap coupled with our ESI source in a more compact design, in which the 90° ion bender is eliminated.[42,43] Coupling the high-resolution PE imaging system with the low temperature ion trap has allowed us to obtain high resolution PE spectra for a number of complex anions produced from our ESI source.[44,45] This new development provides an excellent opportunity for us to accurately measure the EA, as well as vibrational information, of C_{60}. Furthermore, the PE imaging experiment will also yield photoelectron angular distribution (PAD), which can provide additional information about the nature of the occupied molecular orbital (MO) from which the electron is detached.

The PAD of randomly orientated anions for a one-photon detachment process with a linearly polarized light is given by[46]

$$I(\theta) = \sigma/4\pi[1 + \beta P_2(\cos\theta)], \quad (1)$$

where θ is the PE emission angle relative to the laser polarization, σ is the detachment cross section, β is the anisotropy parameter, and $P_2(\cos\theta)$ is the second order Legendre polynomial. The PAD is described by the anisotropy parameter (β), which varies from −1 to 2. Typically, a single-electron model describes reasonably well the experimental observations. For example, for detachment from a pure atomic *s*-orbital, $\beta = 2$, corresponding to an anisotropic PAD with the maximum of intensity parallel with the photodetachment laser polarization (*p*-wave). If photoemission is different from a pure *s*-orbital (*s*+*d* orbital for instance), then partial wave interference can result in $\beta = -1$, corresponding to an anisotropic PAD with the maximum of intensity perpendicular to the detachment laser polarization. Detachment from atomic *p*-orbitals generates partial electron waves with *d* and *s* angular momenta; and usually for high kinetic energy electrons (above 1 eV), β will converge to 0 (isotropic) for pure *s*-wave or 1 for pure *d*-wave. Even though the singly occupied MO (SOMO) of the ground electronic state of C_{60}^- has been commonly assumed to be a *p*-type valence orbital derived from the lowest unoccupied molecular orbital (LUMO) of C_{60}, it has not been directly experimentally confirmed via angular-dependent PES.

Here we report a study of cold C_{60}^- using our newly developed high-resolution PE imaging system coupled with our improved cryogenic ion trap. PE images have been obtained, over a photon energy range from 354.84 to 461.36 nm, for the detachment transition from the ground electronic and vibrational state of C_{60}^- to the ground electronic state of C_{60} with well-resolved vibrational structures. The EA of C_{60} is accurately measured to be 2.6835 ± 0.0006 eV, consistent with all our prior PES measurements at lower resolution. Interestingly, we have observed a total of 16 vibrational peaks for the ground state of C_{60} from the high-resolution PE spectra. All the vibrational peaks are assigned using the known frequencies of C_{60} in the solid state and most of the vibrational frequencies represent the first measurement for gaseous C_{60}. We find that the vibrational frequencies of C_{60} in the gas and solid phases are similar. Many of the observed vibrational excitations are forbidden, but activated via vibronic couplings. Both the photon energy dependent detachment cross sections and the PAD suggest that the SOMO of C_{60}^- is of *s*-character, inconsistent with the common assumption that the LUMO of C_{60} is a *p*-type orbital.

II. EXPERIMENTAL

The experimental apparatus consists of an ESI source,[35] a temperature-controlled cryogenic ion trap,[11,25] a time-of-flight mass spectrometer, and a high-resolution PE imaging system.[40,41] This is an improved version of our original ESI-PES apparatus that consisted of a room-temperature ion trap and a magnetic-bottle PES analyzer.[35] The C_{60}^- anions were produced by electrospray of a solution prepared according to the literature,[47] as also described in our prior ESI-PES studies of C_{60}^-.[8,11] Anions from the ESI source were guided by two radio-frequency (RF) quadrupole ion guides and an RF-only octopole ion guide into a cryogenically cooled three-dimensional Paul trap in a more compact linear configuration without the 90° ion bender, used in our first generation cold trap.[25] Anions were accumulated and cooled via collisions with a He/H_2 (4:1 volume ratio) buffer gas for 0.1 s before being pulsed out into the extraction zone of a time-of-flight mass spectrometer. The lowest temperature our ion trap can achieve is 4.4 K, measured by a thermal couple off the outer wall of the Paul trap. While vibrational hot bands can be completely eliminated at ion trap temperatures much higher than 4.4 K as shown previously,[11] we recently estimated a rotational temperature of 35 K for the uracil anion even when the trap was operated at 4.4 K.[45] The experiment reported in the current study was all done by operating the ion trap at 4.4 K to achieve the best rotational cooling.

The C_{60}^- anions were focused into the co-linear velocity-map imaging system, where anions were photodetached by a linear polarized laser beam. The laser polarization was aligned parallel to the imaging detector. Photoelectrons were accelerated toward a position-sensitive detector with a 75 mm diameter micro-channel plate coupled to a phosphor screen and captured by a charge-coupled device (CCD) camera before being finally sent to a computer. The recorded PE images were corrected, smoothed, and inverse-Abel transformed to obtain three-dimensional electron distributions. This reconstruction was carried out by both the pBASEX[48] and BASEX[49] programs, which yielded similar results. Two laser systems were used in the current experiment: an Nd:YAG laser (354.84 nm, the third harmonic) and a tunable dye laser. It should be noted that the laser intensity was controlled below 25 mJ/cm^2 to balance between direct detachment signals from the cold C_{60}^- and minimization of thermionic emission due to multiphoton absorptions known for C_{60}^-.[6,50] The velocity-map imaging system was calibrated with the PE images of atomic I^- and Au^- (Ref. 51) at several different photon energies. The PE spectra presented in this work are all plotted with respect to the electron binding energies obtained by subtraction of the

measured electron kinetic energies (KE) from the photon energies used. The spectral resolution achieved was 3.8 cm^{-1} at 55 cm^{-1} and about 1.5% ($\Delta E/E$) for KE above 1 eV.

III. RESULTS

A. Photoelectron images and spectra at 354.84 nm and 404.33 nm

Fig. 1 shows the PE images and spectra of C_{60}^- at 404.33 and 354.84 nm and at 4.4 K trap temperature. The images were inverse-Abel transformed using the pBASEX method[48] and the double arrow below the images indicates the polarization of the detachment lasers. It should be pointed out that the weak and narrow rings in the PE image at 354.84 nm (Fig. 1(b)) are artifacts from the inverse-Abel reconstruction due to poor resolution at such high KE. The 354.84 nm image using the third harmonic of the Nd:YAG laser was taken in the current study, in order to compare with the previous PE spectrum of cold C_{60}^- taken with our magnetic-bottle analyzer at a 70 K trap temperature and the same detachment wavelength.[11] The current spectrum is consistent with the previous data, except that the resolution of the current spectrum is slightly lower at this wavelength.

However, at 404.33 nm using the dye laser, the spectrum is significantly better resolved (Fig. 1(a)). The two spectra in Fig. 1 are plotted in the same binding energy range for easy comparison. This spectral range up to ~3.1 eV in binding energy covers the main Franck-Condon active range of the detachment transition from the ground state of C_{60}^- to that of C_{60}.[11] In addition to the better spectral resolution, there are two significant changes in the 404.33 nm spectrum relative to that at 354.84 nm. First, the relative intensity of the 0_0^0 peak, which defines the EA of C_{60}, is dramatically reduced at the lower photon energy. The 0_0^0 transition is the dominant peak in the 354.84 nm spectrum, consistent with the relatively minor geometry changes between the anion and neutral ground state of C_{60}. The 354.84 nm spectrum should represent the Franck-Condon profile for the ground state transition; hence changes of the relative intensities of the different vibrational peaks at 404.33 nm suggest either threshold effects or other resonant effects. Second, there is a low binding energy tail in the 404.33 nm spectrum due to vibrational hot bands. This observation suggests that there must be multiphoton absorption at this wavelength, where some of the absorbed photon energies are converted to the internal energy of the anion before photodetachment. Such hot band signals were observed more prominently in our previous room-temperature PE spectra of C_{60}^-,[8] and were completely eliminated even at the 70 K trap temperature,[11] as can also be seen in the 354.84 nm spectrum (Fig. 1(b)). The significant signals near threshold in the 404.33 nm spectrum (Fig. 1(a)) are most likely due to thermionic emission, consistent with multiphoton absorption. It was shown previously that the thermionic emission could become the dominant electron detachment signals for hot C_{60}^- samples.[6]

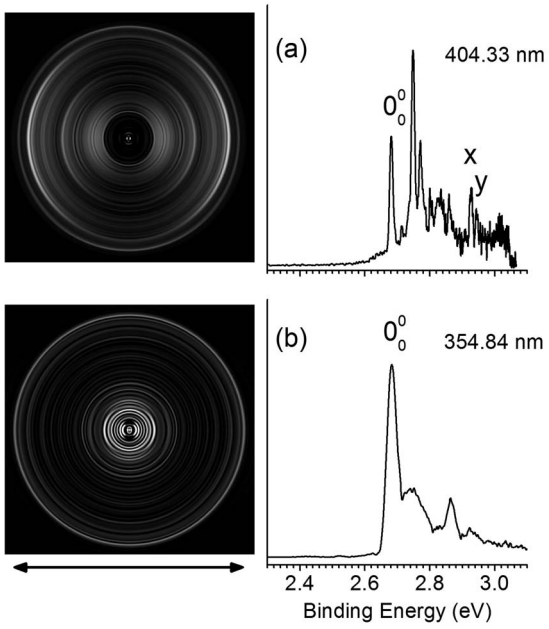

FIG. 1. PE images and spectra of C_{60}^- at (a) 404.33 nm and (b) 354.84 nm and 4.4 K ion trap temperature. The arrows indicate the directions of the laser polarization.

B. Photoelectron images and spectra from 427.16 nm to 452.33 nm

In order to further improve the spectral resolution, we took PE images of cold C_{60}^- at 4.4 K and successively lower detachment photon energies from 427.16 nm to 452.33 nm using a dye laser, as displayed in Fig. 2. The PE images shown in Fig. 2 were again inverse-Abel transformed using the pBASEX method[48] and the double arrow below the images indicates the polarization of the detachment laser. Since the spectral resolution is proportional to the radius of the images, that is, $\Delta E \propto r$ or $KE^{1/2}$, lower photon energies allow the resolution of the low binding energy features to be systematically enhanced.[52] In addition to the 0_0^0 transition, we are able to resolve 16 distinct vibrational peaks up to 2.90 eV binding energy. These peaks are labeled by the lower case letters in Fig. 1 as *x* and *y* and Fig. 2 from *a* to *n*. Because of the complete elimination of vibrational hot bands, all observed peaks should be due to vibrational excitations of the C_{60} ground electronic state. Even very weak peaks can be assigned with confidence, such as peak *d* at 2.7666 eV. The binding energies of all the observed peaks are given in Table I. They are each measured from the best-resolved spectra, i.e., the lowest photon energy that a given feature is observed. For example, the binding energy of peak *c* is measured from the 448.13 nm spectrum (Fig. 2(b)) and that of peak *e* is from the 445.13 nm spectrum (Fig. 2(c)), etc. Peak *c*, which is 0.0659 eV (531 cm^{-1}) above the 0_0^0 transition, is the dominant peak in all the low binding energy spectra from 404.33 nm to 448.13 nm (Fig. 1(a) and Figs. 2(b)–2(f)).

The relative intensities of most of the observed peaks appear to depend on the photon energies. In particular, the intensity of the 0_0^0 peak continues to decrease relative to that of peak *c* as the photon energy decreases. Even though the 0_0^0 transition is the strongest peak relative to the weak peaks *a* and *b* at 452.33 nm (Fig. 2(a)), its detachment cross

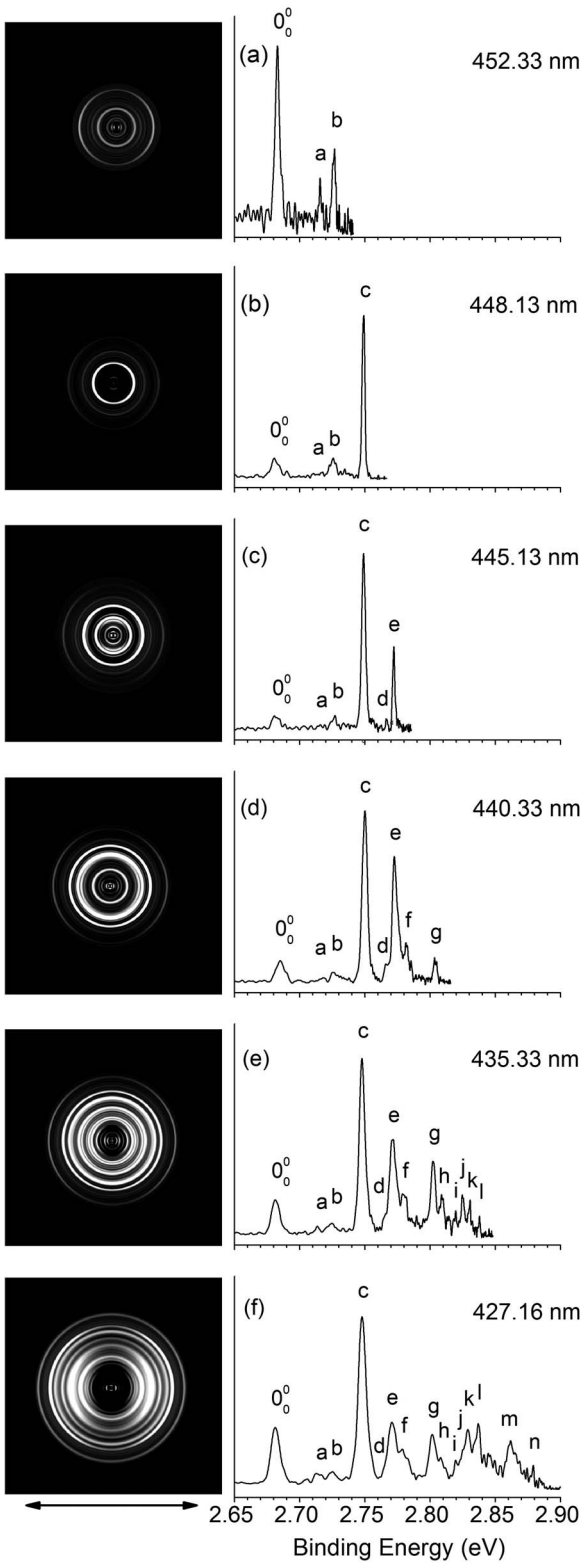

FIG. 2. [(a)–(f)] PE images and spectra of C_{60}^- at six different detachment wavelengths at 4.4 K ion trap temperature. The arrows indicate the directions of the laser polarization.

section is extremely low at this wavelength. As a matter of fact, the spectrum shown in Fig. 2(a) was accumulated for more than 7 h, about three times longer than the other spectra at higher photon energies, in order to get reasonable counting statistics.

C. The photoelectron image and spectrum at 461.36 nm: The precise EA of C_{60}

To obtain the highest resolution for the 0_0^0 transition and the most accurate measurement for the EA of C_{60}, we took the PE image of C_{60}^- at the 4.4 K trap temperature and 461.36 nm, which is barely above the detachment threshold. Fig. 3 shows the obtained PE spectrum at 461.36 nm after inverse-Abel transformation of the PE image using the pBASEX method and then integrating the signals radially. As shown in Fig. 2, the detachment cross section for the 0_0^0 transition decreases with the photon energies and it becomes extremely low at 461.36 nm. Several spectra were measured with very low photon energies. The spectrum shown in Fig. 3 at 461.36 nm was accumulated for more than 6 h. The 0_0^0 peak is well resolved in Fig. 3 and its full width at half maximum (FWHM) is measured to be 10 cm^{-1} at an electron kinetic energy of 31 cm^{-1}. The peak is broader than our instrumental resolution probably due to rotational broadening.[44,45] The EA of C_{60} is accurately defined by this peak as 2.6835 ± 0.0006 eV. The continuous signals present in the region between 2.61 eV and 2.68 eV in Fig. 3 are most likely due to either thermionic emission or hot band transitions as a result of multiphoton absorption, similar to that observed in Fig. 1(a) at 404.33 nm, as well as background noises, because of the long data acquisition time and the low detachment cross section.

IV. DISCUSSION

A. The electron affinity of buckminsterfullerene

The current value of 2.6835 ± 0.0006 eV represents the most accurate measurement for the EA of C_{60} to date. Our PE imaging lens had a resolution of 3.8 cm^{-1} (FWHM) for electrons with 55 cm^{-1} kinetic energies for atomic transitions.[40] The 0_0^0 peak in Fig. 3 corresponds to an electron kinetic energy of 31 cm^{-1}; the instrumental resolution at this kinetic energy should be ~2 cm^{-1}. The observed 10 cm^{-1} peak width should mainly come from rotational broadening. Our recent PE imaging studies on cold phenoxide and deprotonated uracil anions revealed rotational profiles for resolved vibrational peaks.[44,45] Simulations of the rotational profiles resulted in a rotational temperature of 35 K for the uracil anion while the ion trap was operated at 4.4 K.[45] Clearly, the cryogenic ion trap was effective for vibrational cooling, but less so for rotational cooling, probably due to the micro-motion of the ions in the Paul trap and the weak collisions with the background gases. Interestingly, the cooling mechanisms in the cryogenic ion trap is quite different from supersonic expansions, where rotational cooling is highly effective while vibrational cooling is usually less effective due to the unfavorable vibrational to translational energy transfer. In any case, the peak width does not limit the accuracy of determining the positions of the resolved vibrational peaks in the PE images. The 0.0006 eV uncertainty assessed for the 0_0^0 peak in Fig. 3 comes mostly from the size of the CCD camera pixels.

Table II compares the current EA of C_{60} with all the previous measurements and the methods used. It is interesting to note that all the previous PES measurements are consistent with the current accurate value. In particular, our previous

TABLE I. The measured electron binding energies (BE) of the observed vibrational peaks for C_{60}, their shifts relative to the 0_0^0 peak, in comparison with the vibrational frequencies of C_{60} measured in the solid state, and the proposed assignments. The nature of the PAD for the 0_0^0, *c*, and *e* peaks is also indicated.

Observed peak	BE (eV)	Shift (cm^{-1})	Solid C_{60} [a] (cm^{-1})	Assignment[b]	PAD
0_0^0	2.6835(6)	0			*p*
a	2.7160(7)	262	265	$H_g(1)$	
b	2.7267(7)	348	352	$G_u(1)$	
			342	$T_{2u}(1)$	
c	2.7494(7)	531	533	$H_u(2)$	*p*
			527	$T_{1u}(1)$	
d	2.7666(7)	670	666	$H_u(3)$	
e	2.7724(7)	717	712	$T_{2u}(2)$	*s*+*d*
			707	$H_g(3)$	
f	2.7813(12)	789	793	$T_{2g}(3)$	
			784	$G_u(2)$	
g	2.8037(7)	969	974	$T_{2u}(3)$	
			964	$G_u(4)$	
h	2.8094(12)	1015	531 + 484	$H_u(2)/T_{1u}(1)$[c] + $G_g(1)$	
i	2.8192(12)	1094	1092	$G_g(4)$	
j	2.8252(12)	1143	717 + 426	$T_{2u}(2)/H_g(3)$[c] + $H_g(2)$	
k	2.8306(7)	1186	1192	$T_{1u}(3)$	
			1195	$T_{2u}(4)$	
l	2.8380(7)	1246	1251	$H_g(6)$	
m	2.8619(12)	1439	1443	$T_{1u}(4)$	
			1432	$G_u(6)$	
			1430	$H_g(7)$	
n	2.8793(7)	1579	1566	$H_g(8)$	
x	2.928(2)	1972	531 + 1439	$H_u(2)/T_{1u}(1)$[c] + $T_{1u}(4)/G_u(6)/H_g(7)$[c]	
y	2.945(2)	2109	531 + 1578	$H_u(2)/T_{1u}(1)$[c] + $H_g(8)$	

[a]The vibrational frequencies of solid C_{60} measured by INS spectroscopy, IR spectroscopy, and Raman spectroscopy from Ref. 15.
[b]The numbering of each mode is in ascending order of vibrational frequencies, consistent with that used in Refs. 8, 10, and 11.
[c]The frequencies for these modes are from the current work.

PES measurement of 2.683 ± 0.008 eV for cold C_{60}^- was highly accurate,[11] even though the resolution of the magnetic-bottle analyzer used in that experiment was only about 20 meV. For vibrationally resolved peaks, our ability to determine the peak position was not limited by the peak width, as long as the peak shape is well defined with high signal-to-noise ratio. The 0.008 eV uncertainty in that experiment came mainly from the accuracy of the spectral calibration.

Clearly, the EAs reported from the two photodetachment experiments of C_{60}^- in the storage rings were too low.[9,12] In principle, threshold photodetachment of anions should yield highly accurate EAs, if a clear detachment threshold can be observed.[53] There could be two sources of error for the previous storage ring measurements: (1) vibrational hot bands and (2) thermionic emissions. In the first threshold photodetachment experiment on C_{60}^- in 1991,[6] significant photodetachment signals were observed even at photon energies well below the detachment threshold due to thermionic emission as a result of multiphoton absorption. Thermionic emission could dominate the detachment signals if high photon flux was used or if the C_{60}^- anion was hot. A clear rise of detachment signals was observed at 2.60 eV, but a final value of 2.65

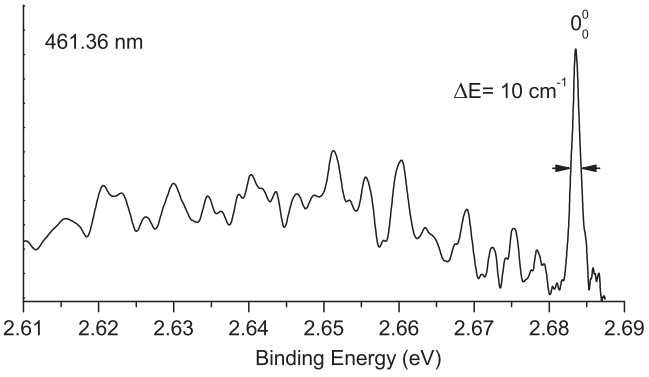

FIG. 3. PE spectrum of C_{60}^- at 461.36 nm at 4.4 K ion trap temperature.

TABLE II. Comparison of the electron affinity measured for C_{60} from the current work with those in the literature. The current work at the bottom is in bold for emphasis on the improvement of our measured electron affinity.

Source	Electron affinity (eV)	Method
Yang *et al.* (Ref. 5)	2.6 – 2.8	PES
Wang *et al.* (Ref. 6)	2.65 ± 0.05	Threshold PD
Brink *et al.* (Ref. 9)	2.666 ± 0.001	Threshold PD
Gunnarsson *et al.* (Ref. 10)	2.70 ± 0.05	PES
Wang *et al.* (Ref. 8)	2.689 ± 0.008	PES at RT
Wang *et al.* (Ref. 11)	2.683 ± 0.008	PES at 70 K
Stochkel *et al.* (Ref. 12)	2.664 ± 0.005	Threshold PD
The current work	**2.6835 ± 0.0006**	

± 0.05 eV was reported.[6] The large uncertainty of 0.05 eV assessed was mainly because of the unknown contributions from vibrational hot bands. In the 1995 photodetachment experiment in the storage ring by Brink *et al.*,[9] the electron count rates were quite low and the signal-to-noise ratios of the electron yield versus photon energies were rather poor. Hence, the EA of 2.666 ± 0.001 eV reported for C_{60} was clearly too low. In the new measurement by Stochkel and Andersen,[12] photodetachment was carried out between 430 and 480 nm with much better electron count rates. Even though the storage ring was cooled to liquid nitrogen temperature, significant signals below threshold were observed. A rise of signal was observed at 465.5 nm and a 1 nm uncertainty was assessed, yielding the reported EA of 2.664 ± 0.005 eV.[12] This value apparently was still too optimistic, even though a larger uncertainty was assessed than the previous storage ring measurement. In light of the current observation that the cross section for the 0_0^0 transition becomes extremely low near threshold, it seems that threshold detachment of C_{60}^- would not be suitable to measure the EA of C_{60} if vibrational hot bands and thermionic emission cannot be completely eliminated.

B. Assignments of the observed vibrational features

In the previous PES measurements,[8,10,11] vibrational structures were only partially resolved for the ground electronic state of C_{60} and they were interpreted qualitatively on the bases of the JT effect and the Franck-Condon principle. With much improved resolution, our original goal in the current work was to resolve the two totally symmetric A_g modes and the eight JT-active H_g modes. In the condensed phase, C_{60} is a weakly interacting molecular solid. Indeed we found that the vibrational frequencies measured for C_{60} in the solid state are quite close to those of isolated C_{60} and can be used to assist our vibrational assignments, as given in Table I. In fact, we found that the vibrational frequencies of the current measurements for gaseous C_{60} are the same as those reported for C_{60} in the condensed phase within the uncertainties of the two different types of experiments. We are able to assign five peaks unambiguously (*a, d, i, l, n*). Six peaks (*b, c, e, f, g, k*) can be assigned to two possible modes with close frequencies, whereas peak *m* can be assigned to three possible modes. Four peaks (*h, j, x, y*) are due to combination modes.

The assignments given in Table I reveal a number of surprises. First, none of the resolved vibrational peaks belong to any of the A_g modes, probably due to unfavorable Franck-Condon factors. This is consistent with the understanding that the C_{60} cage is highly rigid and even the JT-induced atomic displacements are small compared to zero-point motions.[34] Second, not all of the eight H_g modes were observed. For example, the $H_g(2)$ mode with a frequency of 428 cm^{-1} is unambiguously missing in our PE spectra (Fig. 2 and Table I).[15] Among the observed H_g modes (*a, e, j, l, m, n*), only $H_g(3)$ (peak *e*) is likely to have a relatively strong Franck-Condon factor. These observations are not in good accord with theoretical predictions that $H_g(1)$, $H_g(2)$, $H_g(7)$, and $H_g(8)$ are crucial JT-active modes.[26]

C. Observation of forbidden vibrational modes and Hertzberg-Teller coupling

Surprisingly, we observed many forbidden vibrational modes, especially those modes with *u* parity, as seen in Table I. In particular, the dominant peak *c* can be assigned only to $H_u(2)$ or $T_{1u}(1)$ within our resolution, none of which is a JT-active mode in the anion. Therefore, there must be other vibronic coupling effects involved in addition to the JT effect, such as the Hertzberg-Teller (HT) coupling, which involves coupling between two electronic states via non-totally symmetric vibrational modes.[54–57] Extensive HT coupling has been observed recently in high-resolution PE imaging spectroscopy of the C_9H_7 (indenyl) and $C_{13}H_9$ (fluorenyl) anions by Neumark and co-workers.[55] HT coupling is a direct manifestation of the breakdown of the Born-Oppenheimer approximation, which assumes that the electronic motion is independent of the nuclear degrees of freedom. The first-order HT coupling describes two electronic states coupled by a non-totally symmetric vibrational mode. Vibronic coupling is usually effective when the two electronic states are close to each other. But vibronic coupling has been observed for two electronic states that are more than 3 eV apart in the indenyl anion, for example.[55]

We first consider HT coupling in the ground state of C_{60}^- because its first excited electronic state $^2T_{1g}$ is close to its $^2T_{1u}$ ground state (<2 eV).[56] The $T_{1u} \otimes T_{1g}$ coupling can activate vibrational modes with A_u, H_u, and T_{1u} symmetries. We did not observe any vibrational levels of A_u symmetry, but did observe vibrational excitations involving the H_u or T_{1u} modes. For example, the strong peak *c* is assigned to either the $H_u(2)$ or $T_{1u}(1)$ mode, which have similar frequencies (within 6 cm^{-1}) and cannot be distinguished with our experimental accuracy. In fact, the dominant peak *c* may be a strong indication of the HT coupling in the C_{60}^- anion. However, the HT coupling in the anion cannot interpret the observed forbidden vibrational modes with T_{2u}, G_u, and G_g symmetries, which are likely due to HT coupling between the neutral C_{60} ground state (^1A_g) and its excited states. The first two excited open-shell electron configurations of C_{60} are $\ldots h_g^{10} h_u^9 t_{1u}^1$ and $\ldots h_g^{10} h_u^9 t_{1g}^1$, which give rise to *g*-type electronic states (T_{1g}, T_{2g}, G_g, H_g) and *u*-type electronic states (T_{1u}, T_{2u}, G_u, H_u), respectively.[54,56] The electronic states with T_{2u}, G_u, and G_g symmetries are all within 3 eV above the neutral ground state.[56] So vibrational modes of T_{2u}, G_u, and G_g symmetries are allowed via HT coupling between the neutral ground state ^1A_g and the T_{2u}, G_u, or G_g electronic excited states in neutral C_{60}.

D. The relative intensity changes of the vibrational levels with photon energies

We observed that the intensity of the 0_0^0 peak decreases relative to that of peak *c* as the photon energy decreases, as shown in Figs. 1 and 2. From the PAD analyses (Fig. 4 and Table I), both the 0_0^0 and *c* peaks are *p*-wave-like. According to Wigner's threshold law,[58] the detachment cross sections for both peaks should decrease as the photon energies approach the respective detachment threshold. The relative intensity of

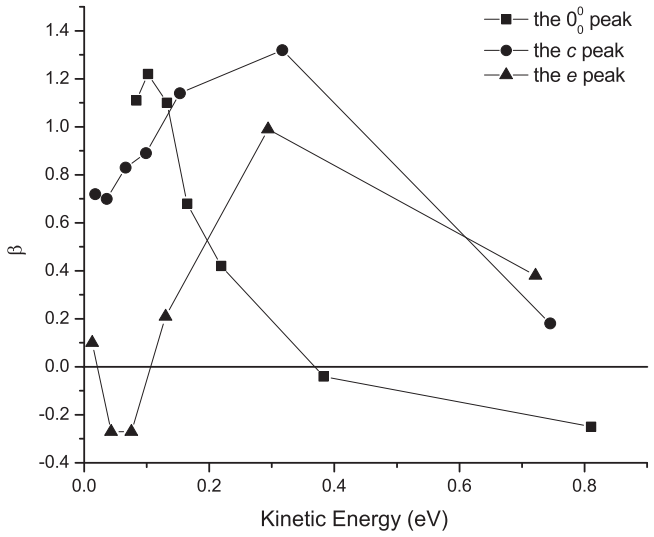

FIG. 4. The anisotropy parameter β as a function of electron kinetic energy for the 0_0^0, *c*, and *e* peaks (see Fig. 2). The horizontal line at $\beta = 0$ is drawn to guide the eyes.

the 0_0^0 peak indeed follows the threshold law, and becomes extremely small near the detachment threshold, as shown in Fig. 3. In contrast, peak *c* does not follow Wigner's threshold law. In all PE spectra, the electron KE of the *c* peak is smaller than that of the 0_0^0 peak. In principle, the threshold law should have more influence on the *c* peak than the 0_0^0 peak. However, the *c* peak remains very strong even at very slow KE, as shown in Fig. 2(b).

The different behaviors of the *c* and 0_0^0 peaks might be another indication of HT coupling. As discussed above, the *c* peak corresponds to either the $H_u(2)$ or $T_u(1)$ mode owing to HT coupling in the anion. Thus, the *c* peak comes from intensity borrowing from the anion excited state and must also carry electronic characters of the excited state, as is also observed in the recent study on the indenyl and fluorenyl anions.[55] The intense *c* peak could also be due to a nuclear-excited Feshbach resonance. In electron attachment experiments on C_{60}, numerous resonances were observed for very low incoming electrons due to both Feshbach and shape resonances.[59–62] These resonances can be accessed conceivably by photoexcitation of the C_{60}^- anion, resulting in the enhanced detachment cross sections.

E. The photoelectron angular distributions

Fig. 4 shows the anisotropy parameter β as a function of electron KE for the three most intense vibrational peaks, 0_0^0, *c*, and *e* peaks. Other vibrational peaks are too weak for us to extract reliable β parameters. In principle, the overall trend of the anisotropy parameter β as a function of electron KE should be similar for the three vibrational levels, because they are all from the same electronic state of C_{60}. However, the PADs of the *c* and *e* peaks are quite different from that of the 0_0^0 peak and from each other. These differences in PADs provide further evidence for the origins of peaks *c* and *e*, which are due to HT couplings. Therefore, not only the intensities can be borrowed from the excited electronic states, but also their electronic characters, via vibronic coupling.[55,63]

The variation of the β value of the 0_0^0 peak with electron KE suggests that it is not due to a pure *s* state. The β of the 0_0^0 peak is positive (>1) near threshold, indicating the outgoing electron is a *p* wave. Hence, the orbital from which the electron is detached in C_{60}^- should be *s*- or *d*-like. The low detachment cross section of the 0_0^0 peak near threshold is also consistent with the *p*-wave character of the outgoing electron on the basis of Wigner's threshold law. However, this observation is not consistent with the common assumption that the LUMO of C_{60}, where the extra electron resides in C_{60}^-, has *p* character because it is composed of *p*-type valence orbitals from carbon.[64,65] On the other hand, scanning tunneling spectroscopy studies of C_{60} adsorbed on surfaces suggest that the π^* LUMO of C_{60} consists of sp^2 hybridized orbitals,[66,67] which are consistent with the s-character for the LUMO revealed from the current study.

V. CONCLUSIONS

We report high-resolution photoelectron imaging of cold C_{60}^- and the most accurate electron affinity of C_{60} as 2.6835 ± 0.0006 eV. Extensive vibrational structures were observed for the ground electronic state of C_{60}, as a result of vibronic couplings in both the anion and neutral ground states. Because of the elimination of vibrational hot bands in the C_{60}^- anion, even very weak vibrational peaks can be assigned on the bases of those observed for solid C_{60}. The vibrational frequencies of the gaseous C_{60} are observed to be very similar to those in the condensed phase within the experimental uncertainties. A total of sixteen vibrational peaks were observed, corresponding to fourteen fundamental vibrational modes of C_{60}, many of which are reported for the first time for gaseous C_{60}. Evidence of vibronic couplings was also observed in both the relative intensity changes and the photoelectron angular distributions. The orbital where the extra electron of C_{60}^- resides is found to be consistent with a *s*-like orbital, in contrast to the common assumption of a *p*-like LUMO for C_{60}.

ACKNOWLEDGMENTS

This work was supported by the National Science Foundation (CHE-1049717).

[1]H. W. Kroto, J. R. Heath, S. C. Obrien, R. F. Curl, and R. E. Smalley, Nature (London) **318**, 162 (1985).
[2]M. Prato, J. Mater. Chem. **7**, 1097 (1997).
[3]H. Park, J. Park, A. K. L. Lim, E. H. Anderson, A. P. Alivisatos, and P. L. McEuen, Nature (London) **407**, 57 (2000).
[4]J. L. Segura, N. Martin, and D. M. Guldi, Chem. Soc. Rev. **34**, 31 (2005).
[5]S. H. Yang, C. L. Pettiette, J. Conceicao, O. Cheshnovsky, and R. E. Smalley, Chem. Phys. Lett. **139**, 233 (1987).
[6]L. S. Wang, J. Conceicao, C. M. Jin, and R. E. Smalley, Chem. Phys. Lett. **182**, 5 (1991).
[7]A. Sassara, G. Zerza, and M. Chergui, J. Phys. B: At. Mol. Opt. Phys. **29**, 4997 (1996).
[8]X. B. Wang, C. F. Ding, and L. S. Wang, J. Chem. Phys. **110**, 8217 (1999).
[9]C. Brink, L. H. Andersen, P. Hvelplund, D. Mathur, and J. D. Voldstad, Chem. Phys. Lett. **233**, 52 (1995).
[10]O. Gunnarsson, H. Handschuh, P. S. Bechthold, B. Kessler, G. Gantefor, and W. Eberhardt, Phys. Rev. Lett. **74**, 1875 (1995).

[11]X. B. Wang, H. K. Woo, and L. S. Wang, J. Chem. Phys. **123**, 051106 (2005).
[12]K. Stochkel and J. U. Andersen, J. Chem. Phys. **139**, 164304 (2013).
[13]K. A. Wang, A. M. Rao, P. C. Eklund, M. S. Dresselhaus, and G. Dresselhaus, Phys. Rev. B **48**, 11375 (1993).
[14]V. Schettino, M. Pagliai, L. Ciabini, and G. Cardini, J. Phys. Chem. A **105**, 11192 (2001).
[15]S. F. Parker, S. M. Bennington, J. W. Taylor, H. Herman, I. Silverwood, P. Albers, and K. Refson, Phys. Chem. Chem. Phys. **13**, 7789 (2011).
[16]J. Menendez and J. B. Page, Top. Appl. Phys. **76**, 27 (2000).
[17]H. Kuzmany, R. Winkler, and T. Pichler, J. Phys.: Condens. Matter **7**, 6601 (1995).
[18]M. S. Dresselhaus, G. Dresselhaus, and P. C. Eklund, J. Raman Spectrosc. **27**, 351 (1996).
[19]R. H. Xie, G. W. Bryant, L. Jensen, J. J. Zhao, and V. H. Smith, J. Chem. Phys. **118**, 8621 (2003).
[20]V. Schettino, P. R. Salvi, R. Bini, and G. Cardini, J. Chem. Phys. **101**, 11079 (1994).
[21]C. H. Choi, M. Kertesz, and L. Mihaly, J. Phys. Chem. A **104**, 102 (2000).
[22]F. Negri and G. Orlandi, J. Phys. B: At. Mol. Opt. Phys. **29**, 5049 (1996).
[23]M. C. Martin, X. Q. Du, J. Kwon, and L. Mihaly, Phys. Rev. B **50**, 173 (1994).
[24]D. A. Jelski, L. Nemes, and S. A. Broughton, J. Cluster Sci. **16**, 1 (2005).
[25]X. B. Wang and L. S. Wang, Rev. Sci. Instrum. **79**, 073108 (2008).
[26]H. Ramanantoanina, M. Gruden-Pavlovic, M. Zlatar, and C. Daul, Int. J. Quantum Chem. **113**, 802 (2013).
[27]N. Iwahara, T. Sato, and K. Tanaka, J. Chem. Phys. **136**, 174315 (2012).
[28]N. Iwahara, T. Sato, K. Tanaka, and L. F. Chibotaru, Phys. Rev. B **82**, 245409 (2010).
[29]F. Negri, G. Orlandi, and F. Zerbetto, Chem. Phys. Lett. **144**, 31 (1988).
[30]I. D. Hands, J. L. Dunn, and C. A. Bates, Phys. Rev. B **82**, 155425 (2010).
[31]V. C. Long, J. L. Musfeldt, K. Kamaras, A. Schilder, and W. Schutz, Phys. Rev. B **58**, 14338 (1998).
[32]I. D. Hands, J. L. Dunn, C. A. Bates, M. J. Hope, S. R. Meech, and D. L. Andrews, Phys. Rev. B **77**, 115445 (2008).
[33]J. L. Dunn, A. J. Lakin, and I. D. Hands, New J. Phys. **14**, 083038 (2012).
[34]S. Tomita, J. U. Andersen, E. Bonderup, P. Hvelplund, B. Liu, S. B. Nielsen, U. V. Pedersen, J. Rangama, K. Hansen, and O. Echt, Phys. Rev. Lett. **94**, 053002 (2005).
[35]L. S. Wang, C. F. Ding, X. B. Wang, and S. E. Barlow, Rev. Sci. Instrum. **70**, 1957 (1999).
[36]X. P. Xing, X. B. Wang, and L. S. Wang, Phys. Rev. Lett. **101**, 083003 (2008).
[37]X. P. Xing, X. B. Wang, and L. S. Wang, J. Phys. Chem. A **114**, 4524 (2010).
[38]C. G. Ning, P. D. Dau, and L. S. Wang, Phys. Rev. Lett. **105**, 263001 (2010).
[39]P. D. Dau, H. T. Liu, J. P. Yang, M. O. Winghart, T. J. A. Wolf, A. N. Unterreiner, P. Weis, Y. R. Miao, C. G. Ning, M. M. Kappes, and L. S. Wang, Phys. Rev. A **85**, 064503 (2012).
[40]I. Leon, Z. Yang, and L. S. Wang, J. Chem. Phys. **138**, 184304 (2013).
[41]Z. Yang, I. Leon, and L. S. Wang, J. Chem. Phys. **139**, 021106 (2013).
[42]P. D. Dau, H. T. Liu, D. L. Huang, and L. S. Wang, J. Chem. Phys. **137**, 064315 (2012).
[43]H. T. Liu, X. G. Xiong, P. D. Dau, Y. L. Wang, D. L. Huang, J. Li, and L. S. Wang, Nat. Commun. **4**, 2201 (2013).
[44]H. T. Liu, C. G. Ning, D. L. Huang, P. D. Dau, and L. S. Wang, Angew. Chem. Int. Ed. **52**, 8976 (2013).
[45]H. T. Liu, C. G. Ning, D. L. Huang, and L. S. Wang, Angew. Chem. Int. Ed. **53**, 2464 (2014).
[46]J. Cooper and R. N. Zare, J. Chem. Phys. **48**, 942 (1968); **49**, 4252 (1968) (Erratum).
[47]R. Subramanian, P. Boulas, M. N. Vijayashree, F. Dsouza, M. T. Jones, and K. M. Kadish, J. Chem. Soc., Chem. Commun. **1994**, 1847.
[48]G. A. Garcia, L. Nahon, and I. Powis, Rev. Sci. Instrum. **75**, 4989 (2004).
[49]V. Dribinski, A. Ossadtchi, V. A. Mandelshtam, and H. Reisler, Rev. Sci. Instrum. **73**, 2634 (2002).
[50]K. Hansen, J. U. Andersen, H. Cederquist, C. Gottrup, P. Hvelplund, M. O. Larsson, V. V. Petrunin, and H. T. Schmidt, Eur. Phys. J. D **9**, 351 (1999).
[51]H. T. Liu, Y. L. Wang, X. G. Xiong, P. D. Dau, Z. A. Piazza, D. L. Huang, C. Q. Xu, J. Li, and L. S. Wang, Chem. Sci. **3**, 3286 (2012).
[52]D. M. Neumark, J. Phys. Chem. A **112**, 13287 (2008).
[53]H. Hotop and W. C. Lineberger, J. Phys. Chem. Ref. Data **14**, 731 (1985).
[54]S. Leach, M. Vervloet, A. Despres, E. Breheret, J. P. Hare, T. J. Dennis, H. W. Kroto, R. Taylor, and D. R. M. Walton, Chem. Phys. **160**, 451 (1992).
[55]J. B. Kim, M. L. Weichman, T. I. Yacovitch, C. Shih, and D. M. Neumark, J. Chem. Phys. **139**, 104301 (2013).
[56]G. Orlandi and F. Negri, Photochem. Photobiol. Sci. **1**, 289 (2002).
[57]G. J. Small, J. Chem. Phys. **54**, 3300 (1971).
[58]E. P. Wigner, Phys. Rev. **73**, 1002 (1948).
[59]O. Elhamidi, J. Pommier, and R. Abouaf, J. Phys. B: At. Mol. Opt. Phys. **30**, 4633 (1997).
[60]J. Huang, H. S. Carman, and R. N. Compton, J. Phys. Chem. **99**, 1719 (1995).
[61]T. Jaffke, E. Illenberger, M. Lezius, S. Matejcik, D. Smith, and T. D. Mark, Chem. Phys. Lett. **226**, 213 (1994).
[62]M. Lezius, P. Scheier, and T. D. Mark, Chem. Phys. Lett. **203**, 232 (1993).
[63]P. Roy, R. J. Bartlett, W. J. Trela, T. A. Ferrett, A. C. Parr, S. H. Southworth, J. E. Hardis, V. Schmidt, and J. L. Dehmer, J. Chem. Phys. **94**, 949 (1991).
[64]Y. Kitagawa, Y. Nakanishi, T. Saito, K. Koizumi, M. Shoji, S. Yamada, T. Kawakami, M. Okumura, and K. Yamaguchi, Polyhedron **28**, 1750 (2009).
[65]S. Klaiman, E. V. Gromov, and L. S. Cederbaum, J. Phys. Chem. Lett. **4**, 3319 (2013).
[66]X. Lu, M. Grobis, K. H. Khoo, S. G. Louie, and M. F. Crommie, Phys. Rev. B **70**, 115418 (2004).
[67]M. Feng, J. Zhao, and H. Petek, Science **320**, 359 (2008).